Current Optics and Photonics
Vol. 2, No. 6, December 2018, pp. 519-524

ISSN: 2508-7266(Print) / ISSN: 2508-7274(Online)
DOI: https://doi.org/10.3807/COPP.2018.2.6.519

A Transverse Load Sensor with Reconfigurable Measurement Accuracy Based on a Microwave Photonic Filter

Han Chen*, Changqing Li, and Jing Min

School of Instrument Science and Engineering, Southeast University, Nanjing 210096, People's Republic of China

(Received April 28, 2018 : revised October 1, 2018 : accepted October 14, 2018)

We propose a transverse load sensor with reconfigurable measurement accuracy based on a microwave photonic filter in the K_u band, incorporating a polarization-maintaining fiber Bragg grating. A prototype sensor with a reconfigurable measurement accuracy tuning range from 6.09 to 9.56 GHz/(N/mm), and corresponding minimal detectable load range from 0.0167 to 0.0263 N/mm, is experimentally demonstrated. The results illustrate that up to 40% manufacturing error in the grating length can be dynamically calibrated to the same corresponding measurement accuracy for the proposed transverse load sensor, by controlling the semiconductor optical amplifier's injection current in the range of 154 to 419 mA.

Keywords : Fiber optics sensors, Filters, Fiber Bragg gratings, Semiconductor optical amplifiers
OCIS codes : (060.2370) Fiber optics sensors; (350.2460) Filters; (060.3735) Fiber Bragg gratings; (250.5980) Semiconductor optical amplifiers

I. INTRODUCTION

Microwave photonics (MWP), focusing on the generation, processing and transport of signals in the far infrared, terahertz, microwave, and ultrahigh-frequency radio domains by photonics, offers many prominent advantages over classical radio frequency (rf) techniques [1]. An important application of MWP is the microwave photonic filter (MPF) [2], which has attracted considerable interest over the past decades thanks to beneficial features such as being wide-band, electromagnetic shielding, tunable, and lightweight [3]. Recently, we have also proposed an ultrawide-band MPF and demonstrated its high quality factor *Q* [4]. Besides the abovementioned distinct features for rf/optical signals [5, 6], MPFs have also been rapidly developed in emerging techniques for sensing, measurement, and detection [7, 8]. A lot of designs, especially those MWP schemes incorporating a fiber Bragg grating (FBG), have already been demonstrated to measure target parameters or signals, including transverse load [9, 10], hydraulic pressure [11], temperature [12], vibration [13], strain/length [14].

Unlike optoelectronic oscillator (OEO) -based approaches in [10, 14], we propose a MPF structure for converting transverse load to a spectrum-filtering signal. This method avoids the measurement of frequency generation in the OEO schemes, and suppresses the measurement error coming from the drift in oscillating frequency due to the influence of environment temperature and vibration on the oscillatory cavity (*i.e.* optical fiber loops exceeding several kilometers in length). Prominent features such as ultrahigh sensitivity, compactness, and multiplexing capability lend FBG-based sensors to a large number of applications, including the measurement of transverse load; however, the measurement curves need to be further calibrated, due to the individual differences in each FBG manufacturing process. Furthermore, the measurement accuracy cannot be reconfigured, even for different application scenarios.

For these reasons, we propose a reconfigurable transverse load sensor based on our previous work [4], in a MPF incorporating a semiconductor optical amplifier (SOA). The proposed MPF along orthogonal polarization in an active loop operates at frequencies up to the K_u band, and

*Corresponding author: hanchen@seu.edu.cn, ORCID 0000-0002-5858-9554
Color versions of one or more of the figures in this paper are available online.

provides a tunable free spectral range (FSR) from 15.44 to 19.44 GHz by control of the SOA's injection current. A prototype of the equivalent second-order infinite-impulse response filter, with a Q factor greater than 6300 and a rejection ratio exceeding 41 dB, is experimentally demonstrated. The involved MPF shows flexible tunability in the K_u band, based on the birefringence effects [15] by controlling the carrier density within the SOA's active region, and it is the tunability of this MPF that allows calibration of the measurement error induced by polarization-maintaining FBGs (PM-FBG), and the compensation for individual differences in each PM-FBG manufacturing process.

In this paper, a prototype sensor with a reconfigurable measurement accuracy tuning range from 6.09 to 9.56 GHz/(N/mm), and corresponding minimum detectable load range from 0.0167 to 0.0263 N/mm, is experimentally demonstrated. These mentioned tunability advantages can also be used to compensate for transverse load sensor errors, for example, even if the FBG length difference is up to 40%.

II. PRINCIPLE

The PM-FBG works as a transverse load sensor. When a transverse force is applied to the PM-FBG it will be birefringent, due to differing refractive indices along the orthogonal directions. The load-induced birefringence B of the PM-FBG is given by [16]

$$B = 2n_0^3(p_{11} - p_{12})(1 + v_p)\cos(2\phi)F/\pi rE \tag{1}$$

where E is the Young's modulus of the fiber, r is the radius of the fiber, F is the linear transverse load per unit length, ϕ is the angle between the direction of the force and the polarization axis of the fiber, v_p is Poisson's ratio, p_{11} and p_{12} are the components of the strain-optical tensor of the optical material, and n_0 is the refractive index for the single-mode fiber (SMF). The differential delay time induced by the PM-FBG $\triangle\tau_1$ is given by

$$\triangle\tau_1 = t_{TE}^1 - t_{TM}^1 = 1/c \cdot L \cdot B \tag{2}$$

where t_{TE}^1 and t_{TM}^1 are respectively the delay time along transverse magnetic (TM) and transverse electric (TE) polarization directions in the PM-FBG, $c = 2.9979 \times 10^8$ m/s is the speed of light in vacuum, $L = 10.0$ cm is the grating length of the PM-FBG, and considering the typical values for an SMF of $n_0 = 1.45$, $p_{11} = 0.12$, $p_{12} = 0.27$, $v_p = 0.17$, $E = 7.6 \times 10^4$ N/mm^2, $r = 62.5$ μm, $\phi = 90°$, the relationship between the induced differential delay time and the transverse load is given by $(d\triangle\tau_1)/dF = 23.67$ ps/(N/mm). Finally, this load-induced birefringence means that the orthogonal parts of a signal pulse travel with different velocities, causing tapped delaying of the proposed infinite-impulse response (IIR) filter.

The SOA works as a tunable birefringence compensator. Its birefringence effects contain a dynamic component and an intrinsic component. The former is determined by the operating state, and the latter is produced by the waveguide's structure and material. When launch power or injection current is applied to the SOA, the change in the carrier density, rather than cross-gain modulation (XGM) effects [17], causes the orthogonal polarization signals to propagate at different group velocities and induce controllable, different delay times along the orthogonal directions. Thus, the total delay time of the proposed IIR filter along TE and TM polarization directions t_{TE} and t_{TM} is given by

$$t_{TE} = t_{TE}^1 + t_{TE}^2;\ t_{TM} = t_{TM}^1 + t_{TM}^2 \tag{3}$$

where t_{TE}^2 and t_{TM}^2 are respectively the delay time along the TM and TE polarization direction in the SOA. The proposed MPF transfer function T can be expressed as the vector sum of the two parallel first-order IIR responses T_{TE} and T_{TM} along the TE and TM polarization directions in the fiber loop, which is theoretically equivalent to a second-order IIR filter,

$$\begin{aligned} T(\omega) &= T_{TE}(\omega) + T_{TM}(\omega) \\ &= 1/(1 - A_{TE} \cdot e^{-j\omega t_{TE}}) + 1/(1 - A_{TM} \cdot e^{-j\omega t_{TM}}) \end{aligned} \tag{4}$$

where A_{TE} and A_{TM} are the transmission coefficients along the TE and TM polarization directions in the fiber loop, which depend on the optical loss coefficient of the VOA, the effective gain of the SOA, and the coupling ratio of the coupler. The differential delay time $\triangle\tau_2$ induced by the SOA is given by

$$\triangle\tau_2 = t_{TE}^2 - t_{TM}^2 \tag{5}$$

$\triangle\tau_2$ is of the order of picoseconds for a SOA with a cavity length of about 1000 μm. For instance, by controlling the SOA injection current I_{inject} [4], measured values are given by $\triangle\tau_2 = 51$ ps $@I_{inject} = 154$ mA and $\triangle\tau_2 = 65$ ps $@I_{inject} = 419$ mA, without considering the differential delay time induced by the PM-FBG.

III. EXPERIMENTAL SETUP

The schematic diagram of the proposed transverse load sensor based on a MPF is shown in Fig. 1. The output of a 1552-nm distributed-feedback (DFB) laser is modulated by a swept rf signal from a vector network analyzer (VNA), using a Mach-Zehnder modulator (MZM) with a 3-dB electrical bandwidth of 20 GHz. The modulated optical signal is sent to an erbium-doped fiber amplifier (EDFA)

and a variable optical attenuator (VOA) to control the launch power, and a polarization controller (PC) afterward is used to generate two orthogonal polarization components along the TE and TM polarization directions. Then the orthogonal polarization signal is split into two paths by a 50:50 coupler via a circulator. One path is reflected from a PM-FBG, which is directly written in a 12-day hydrogen-loaded (10 Mpa @ 24°C) germanium-doped PM fiber and has 99% reflectivity. In the experiment, two kinds of PM-FBGs produced by different types of PM fiber are used, which have different lengths (marked as PM-FBG1, with 10.0 cm length, and PM-FBG2, with 6.0 cm length). The PM-FBG works as a transverse load sensor, which is placed between two glass plates, to which the transverse force is applied, as shown in the lower right corner of Fig. 1. The other path goes into a single active loop consisting of a Fabry-Pérot SOA (FP-SOA) and a VOA. The SOA works as a tunable birefringence compensator and an amplifier to compensate for the loss in the loop. The delay time corresponding to the loop length is larger than the coherence time of the input laser, so that the structure is operated in an incoherent regime. A VOA afterward is used to maintain the optical power in the loop. Then the amplified orthogonal polarization signal is divided into two parts again by the coupler; one is sent to the circulator, and the other will reenter the loop to be delayed and obtain subsequent recursive taps. Thus, the orthogonal polarization signal circulating in the loop realizes two parallel first-order IIR filters with positive coefficient, after passing through a 45° polarizer and a photodetector (PD) incorporated with an optional electronic amplifier (EA).

The measurement shows that the loop length (not including the FP-SOA) of the prototype is about 1.25 m, and the corresponding delay time t is about 6.25 ns (on the order of nanoseconds). Considering $\triangle\tau_1+\triangle\tau_2 \ll t$ from (2) and (5), when the transverse load F is applied, the FSR of the equivalent second-order IIR f_{FSR}^{F} responds as

$$f_{FSR}^{F}=1/(\triangle\tau_1+\triangle\tau_2) \tag{6}$$

Comparing those normal first-order IIR structured MPFs to the FSR less than 200 MHz (corresponding loop length is more than 1 m, due to pigtailed devices), the FSR of the proposed MPF is significantly increased to several GHz, in the K_u band. For instance, when $F=0.1$ N/mm, the theoretical value is given by $f_{FSR}^{0.1}=14.84$ GHz $@I_{inject}=$ 419 mA.

Benefiting from convenient control of the operating state of the FP-SOA, the transverse load sensor based on the proposed IIR filter affords a reconfigurable measurement accuracy. The FP-SOA can also works as a dynamic calibrator unit to compensate for individual length differences due to the manufacturing process of the PM-FBG. Thus the obtained sensing information from the PM-FBG is converted from the optical domain to the electrical domain, which can be directly detected by an electronic spectrum analyzer (ESA).

IV. RESULTS AND DISCUSSIONS

First, the MPF response without transverse load ($F=0$ N/mm) is experimentally demonstrated. Figure 2 shows that the measured MPF center frequency $f_{FSR}^{F}=f_{FSR}^{0}$ is within the range from 15.44 to 19.44 GHz as the FP-SOA injection current is decreased from 419 to 154 mA. In theory, the response should be a comb curve; however, limited by the bandwidth of MZM, PD, EA, etc., the comb filter-response presents as a single passband in the K_u band. For instance, when the FP-SOA injection current I_{inject} is set to 154 mA, the measured values via the VNA (Agilent E8364A) show that the MPF response has a 3-dB bandwidth of less than 2.45 MHz, and a rejection ratio of over 41 dB. The minimal spectrum interval from the peak to the side lobe nearby, or the intervals between the side lobes $\triangle f_{\min}$, is about 160 MHz (1/6.25 ns), in accord

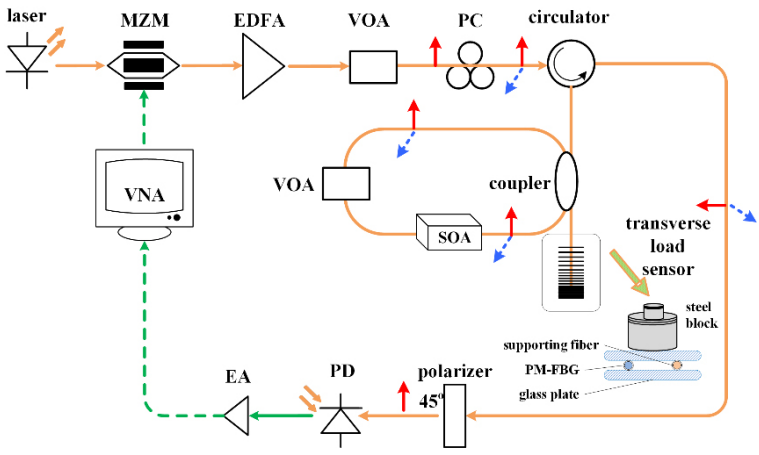

FIG. 1. Experimental setup for the transverse load sensor based on a MPF.

with the 1.25-m fiber loop length of the prototype. These results illustrate that adjusting the central frequency of the passband neither changes the shape of the frequency response, nor degrades the rejection ratio.

Secondly, the reconfigurable transverse-load measurement accuracy is experimentally demonstrated. Figure 3 shows that the MPF's center-frequency offset $f_{offset}^{F} = f_{FSR}^{F} - f_{FSR}^{0}$ is within a range of 1.0 GHz as the transverse load increases from 0 to 0.1 N/mm, when the FP-SOA injection current is set as shown in Fig. 2. The measured values are presented groups of squares in different colors in Fig. 3, and the slope of the corresponding linear fitting is in the range from -6.09 to -9.56. The absolute value of this slope is the proposed sensor's measurement accuracy, which is in the range from 6.09 to 9.56 GHz/(N/mm). For instance, when f_{offset}^{F} changes from 0.44 to 0.60 GHz, *i.e.* $\triangle f_{center} = \triangle f_{\min} = 0.16$ GHz, the corresponding minimal detectable loads are given by $\triangle F_1 = 0.0167$ N/mm $@I_{inject} = 154$ mA, $\triangle F_2 = 0.0263$ N/mm $@I_{inject} = 419$ mA, which are reconfigurable and can be further improved by reducing $\triangle f_{\min}$, *i.e.* lengthening the fiber loop of the prototype.

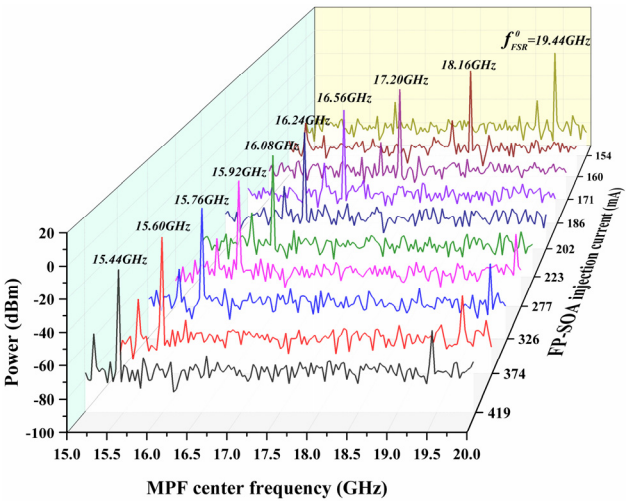

FIG. 2. Measured tunable MPF response without transverse load, by controlling the FP-SOA injection current.

Although this accuracy is acceptable, the degradation is, indeed, obvious. The degradation is due to the increase of injection current in the SOA, and whether the accompanying SOA is working in the saturated state. The results illustrate that an injection current of 250 mA is the turning point of the SOA's gain [4]. Exceeding this value, the SOA operates in the saturated regime. The FSR frequency keeps falling but gradually slows, as the SOA gain observably degrades. This results in an obvious degradation, from 0.0167 N/mm to 0.0263 N/mm, of the measurement accuracy based on FSR. Analysis shows that the reconfigurable ratio $R = (\triangle F_2 - \triangle F_1)/\triangle F_2$ is not less than 40%, which illustrates that adjusting the FP-SOA injection current induces a reconfigurable transverse-load measurement accuracy.

The experimental results mentioned above are obtained when using PM-FBG1; next, PM-FBG2 with a different length (about 6.0 cm) is further used, to demonstrate the dynamic calibration performance for the proposed transverse load sensor. The difference in length between the two PM-FBGs can be regarded as the main source of manufacturing error, which is more than 40% here (but will not be so large in most real-world situations). Figure 4 shows the measured dynamic calibration curve as the transverse load increases from 0 to 0.1 N/mm, when the FP-SOA injection current is set to 419 mA. As an example, for PM-FBG1, when $F = 0.1$ N/mm the measured MPF center frequency $f_{FSR}^{0.1} = 14.91$ GHz, which agrees well with the previous theoretical value $f_{FSR}^{0.1} = 14.84$ GHz. The results illustrate that the slope of the linear fitting curve according to the MPF center frequency is -6.09 for PM-FBG1 (black line) and

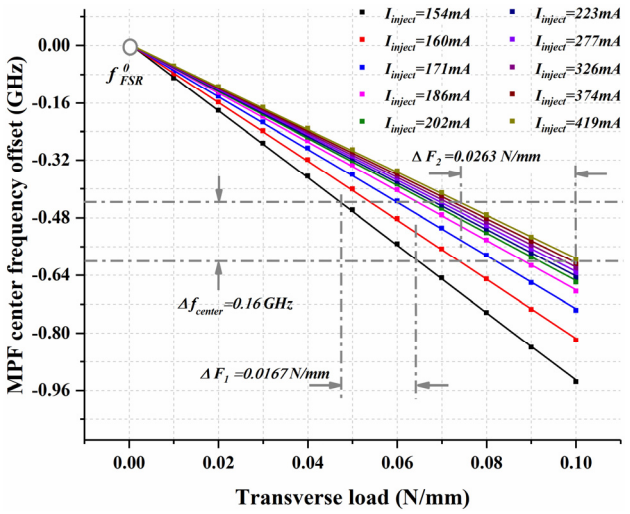

FIG. 3. Measured reconfigurable transverse-load measurement accuracy, by controlling the FP-SOA injection current.

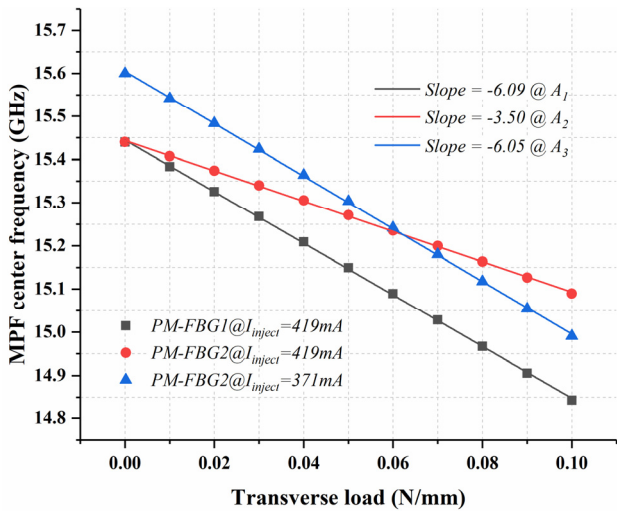

FIG. 4. Measured dynamic calibration curve, when the initial FP-SOA injection current is set to 419 mA.

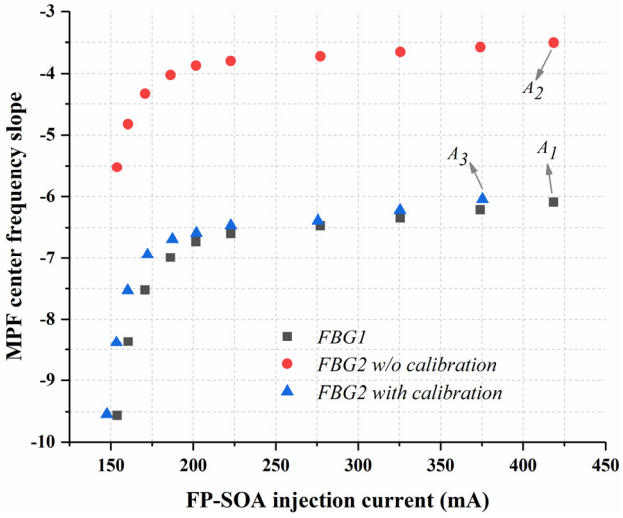

FIG. 5. Measured dynamic calibration for the transverse load sensor, by controlling the FP-SOA injection current.

-3.50 for PM-FBG2 (red line). The values are obviously different and induce a different transverse-load measurement accuracy, which should be calibrated in applications. The calibration curve (blue line) presents a dynamic method to compensate for the measurement accuracy, by decreasing the initial FP-SOA injection current from 419 to 371 mA, and the slope of the calibration curve is measured to be -6.05, close to the initial value -6.09 for PM-FBG1. Thus up to 40% manufacturing error of the grating length can be dynamically calibrated to the same measurement accuracy.

Furthermore, other calibrated FP-SOA injection currents for PM-FBG2 are experimentally demonstrated. Figure 5 shows the measured dynamic calibration for the transverse load sensor while controlling the FP-SOA injection current in the range from 154 to 419 mA; here all of the results shown in Fig. 4 can be condensed into points A_1, A_2, and A_3 in Fig. 5. The results illustrate that the slope of the MPF center frequency with transverse load for the compensated PM-FBG2 (blue triangles) agrees well with the corresponding value for PM-FBG1 (black squares), so the initial measurement accuracy for the sensor incorporating PM-FBG2 (red circles) are properly calibrated.

V. CONCLUSION

In this paper, an experimental investigation of a MPF-based transverse load sensor has been presented. An SOA is used to improve the performances of those traditional transverse load sensors incorporating FBGs, in aspects such as reconfigurable measurement accuracy and compensable error. By controlling the SOA's injection current in the range from 154 to 419 mA, a prototype sensor with a reconfigurable measurement accuracy ranging from 6.09 to 9.56 GHz/(N/mm), and corresponding minimal detectable load ranging from 0.0167 to 0.0263 N/mm, is experimentally demonstrated. Considering the actual manufacturing error of the grating length, the same control method is also proved to be feasible for compensating to the same measurement accuracy of the transverse load sensor, for FBGs of different lengths, and the results illustrate that up to 40% manufacturing error in grating length can be dynamically calibrated.

ACKNOWLEDGMENT

This study was supported by a grant from the National Natural Science Foundation of China (61471116, 61101019).

REFERENCES

1. J. Capmany and D. Novak, "Microwave photonics combines two worlds," Nat. Photon. **1**, 319-330 (2007).
2. J. P. Yao, "Microwave photonics," J. Lightw. Technol. **27,** 314-335 (2009).
3. J. Mora, L. R. Chen, and J. Capmany, "Single-bandpass microwave photonic filter with tuning and reconfiguration capabilities," J. Lightw. Technol. **26**, 2663-2670 (2008).
4. H. Chen, "Ultrawideband microwave photonic filter with high Q-factor using a semiconductor optical amplifier," Opt. Lett. **42**, 1397-1399 (2017).
5. K. Lee, J. H. Lee, and S. B. Lee, "Tunable photonic microwave notch filter using SOA-based single-longitudinal mode, dual-wavelength laser," Opt. Express **17**, 13216-13221 (2009).
6. J. Mora, B. Ortega, A. Díez, J. L. Cruz, M. V. Andrés, J. Capmany, and D. Pastor, "Photonic microwave tunable single-bandpass filter based on a Mach-Zehnder interferometer," J. Lightw. Technol. **24**, 2500-2509 (2006).
7. S. Zhang, R. Wu, H. Chen, H. Fu, J. Li, L. Zhang, M. Zhao, and D. Zhang, "Fiber-optic sensing interrogation system for simultaneous measurement of temperature and transversal loading based on a single-passband RF filter," IEEE Sensors J. **17**, 2036-2041 (2017).
8. H. Fu, W. Zhang, C. Mou, X. Shu, L. Zhang, S. He, and I. Bennion, "High-frequency fiber Bragg grating sensing interrogation system using sagnac-loop-based microwave photonic filtering," IEEE Photon. Technol. Lett. **21**, 519-521 (2009).
9. X. Chen, R. Wu, and H. Fu, "A sensing system for simultaneous measurement of temperature and transversal loading based on a fiber-ring microwave photonic filter," in *Proc. 2017 16th International Conference on Optical Communications and Networks (ICOCN)* (China, Aug. 2017), pp. 1-3.
10. F. Kong, W. Li, and J. Yao, "Transverse load sensing based on a dual-frequency optoelectronic oscillator," Opt. Lett. **38**, 2611-2613 (2013).
11. Y. Gu, Y. Zhao, R. Lv, and Y. Yang, "A practical FBG sensor based on a thin-walled cylinder for hydraulic pressure measurement," IEEE Photon. Technol. Lett. **28**, 2569-2572 (2016).

12. S. Zhang, H. Chen, and H. Fu, "Fiber-optic temperature sensor using an optoelectronic oscillator," in *Proc. 2015 14th International Conference on Optical Communications and Networks (ICOCN)* (China, July 2015), pp. 1-3.
13. Y. Zhu, B. Cong, H. Jiao, X. Jin, H. Chi, S. Zheng, and X. Zhang, "Demodulation of an OEO based vibration sensor with Hilbert Huang Transform," in *Proc. 2015 14th International Conference on Optical Communications and Networks (ICOCN)* (China, July 2015), pp. 1-4.
14. X. Zou, M. Li, W. Pan, B. Luo, L. Yan, and L. Shao, "Optical length change measurement via RF frequency shift analysis of incoherent light source based optoelectronic oscillator," Opt. Express **22**, 11129-11139 (2014).
15. P. Honzatko, A. Kumpera, and P. Skoda, "Effects of polarization dependent gain and dynamic birefringence of the SOA on the performance of the ultrafast nonlinear interferometer gate," Opt. Express **15**, 2541-2547 (2007).
16. B. Guan, L. Jin, Y. Zhang, and H. Tam, "Polarimetric heterodyning fiber grating laser sensors," J. Lightw. Technol. **30**, 1097-1112 (2012).
17. J. Mora, A. Martinez, M. D. Manzanedo, J. Capmany, B. Ortega, and D. Pastor, "Microwave photonic filters with arbitrary positive and negative coefficients using multiple phase inversion in SOA based XGM wavelength converter," Electron. Lett. **41**, 53-54 (2005).